Geophysical Journal International

Geophys. J. Int. (2012) **190,** 230–242 doi: 10.1111/j.1365-246X.2012.05510.x

Relating the permeability of quartz sands to their grain size and spectral induced polarization characteristics

Kristof Koch,[1] André Revil[2,3] and Klaus Holliger[1]

[1] *Institute of Geophysics, University of Lausanne, Amphipole Building,* CH-1015 *Lausanne, Switzerland. E-mail: krs1000@gmail.com*
[2] *Department of Geophysics, Colorado School of Mines, Green Center,* 1500 *Illinois Street, Golden, CO* 80401*, USA*
[3] *ISTerre, CNRS, UMR* 5559, *Université de Savoie, Equipe Volcan,* 73376 *Le Bourget du Lac, France*

Accepted 2012 April 17. Received 2012 April 17; in original form 2011 June 24

SUMMARY

Recently, Revil & Florsch proposed a novel mechanistic model based on the polarization of the Stern layer relating the permeability of granular media to their spectral induced polarization (SIP) characteristics based on the formation of polarized cells around individual grains. To explore the practical validity of this model, we compare it to pertinent laboratory measurements on samples of quartz sands with a wide range of granulometric characteristics. In particular, we measure the hydraulic and SIP characteristics of all samples both in their loose, non-compacted and compacted states, which might allow for the detection of polarization processes that are independent of the grain size. We first verify the underlying grain size/permeability relationship upon which the model of Revil & Florsch is based and then proceed to compare the observed and predicted permeability values for our samples by substituting the grain size characteristics by corresponding SIP parameters, notably the so-called Cole-Cole time constant. In doing so, we also asses the quantitative impact of an observed shift in the Cole-Cole time constant related to textural variations in the samples and observe that changes related to the compaction of the samples are not relevant for the corresponding permeability predictions. We find that the proposed model does indeed provide an adequate prediction of the overall trend of the observed permeability values, but underestimates their actual values by approximately one order-of-magnitude. This discrepancy in turn points to the potential importance of phenomena, which are currently not accounted for in the model and which tend to reduce the characteristic size of the prevailing polarization cells compared to the considered model, such as, for example, membrane polarization, contacts of double-layers of neighbouring grains, and incorrect estimation of the size of the polarized cells because of the irregularity of natural sand grains.

Key words: Electrical properties; Hydrogeophysics; Permeability and porosity.

1 INTRODUCTION

One of the basic difficulties in groundwater resources management is the inherently elusive nature of the spatial distribution of the pertinent hydraulic properties in general and of the permeability in particular (e.g. Gelhar 1993). An adequate hydrological characterization of the subsurface, notably with regard to its permeability structure, is, however, a prerequisite for effectively addressing problems regarding groundwater flow and contaminant transport (e.g. Domenico & Schwartz 1998). Surface- and borehole-based geophysical measurements allow for imaging the geological structure of the shallow subsurface as well as the distribution of some pertinent rock physical properties (e.g. Rubin & Hubbard 2005; Linde *et al.* 2006; Robinson *et al.* 2008; Hubbard & Linde 2011). Geophysical approaches also have the potential of bridging the inherent gap in terms of spatial resolution and coverage that tends to exist for classical hydrological measurements (e.g. Koch *et al.* 2009). Although a number of standard geophysical methods exhibit a direct sensitivity to the water content, such as ground-penetrating radar (e.g. Annan 2005), or to ground water flow, such as self-potential (e.g. Malama *et al.* 2009a,b), only a few methods, such as nuclear magnetic resonance (e.g. Stingaciu *et al.* 2010), seem to exhibit a more or less direct sensitivity to permeability (e.g. Hubbard & Linde 2011). Amongst the latter, spectral induced polarization (SIP) measurements seem to offer particularly significant potential with regard to a wide range of practical hydrological applications (e.g. Slater 2007).

SIP is a low-frequency geoelectrical method based on the observation of effects related to the temporary storage of electrical charges in the probed subsurface region in response to the injection of an alternating current. This reversible storage of electrical charges produces a phase lag between the current injected using two

current electrodes and the voltage difference measured between two potential electrodes (e.g. Binley & Kemna 2005). A number of researchers have tried to connect the key parameters describing the observed SIP phase spectra to various textural characteristics of porous media, which in turn tend to be more or less strongly related to the permeability. Indeed, several studies have documented reasonably strong relationships between permeability and parameters derived from induced polarization (IP) measurements in porous media (e.g. Börner *et al.* 1996; Slater & Lesmes 2002; Kemna *et al.* 2004; Binley *et al.* 2005; Hördt *et al.* 2007; Slater 2007; Revil & Florsch 2010; Weller *et al.* 2010). Slater (2007) provides a comprehensive review of the corresponding methodological foundations and of the pertinent literature. Arguably, the most important textural characteristics in the given context are (i) the pore size or the raw moments of pore size distribution (e.g. Kormiltsev 1963; Titov *et al.* 2002, 2004; Revil *et al.* 2011) and (ii) the grain size or the raw moments of the grain size distributions (e.g. Schwarz 1962; Lesmes & Morgan 2001; Revil & Florsch 2010).

At low frequencies, IP- and SIP-type phenomena are related to the existence of polarization length scales associated with the accumulation or depletion of charge carriers, notably ions in the case of saturated porous media, under the effect of an imposed electrical field. If, and only if, these polarization length scales can be associated with the geometrical parameters controlling permeability, then IP- or SIP-type measurements over a broad range of frequencies, typically 1–100 Hz, can be used to assess permeability. Schwarz (1962) developed the theoretical foundations for linking the diameter of suspended spheres with the relaxation time. This theoretical framework was adapted by Leroy *et al.* (2008) to account for polarization processes in the Stern layer formed by counterions, which maintain their hydration shells and are weakly sorbed to the mineral surface. Revil & Florsch (2010) then proposed a mechanistic theory to predict the permeability of granular media from some raw moments of the grain size distribution and the intrinsic formation factor corrected for surface conductivity. This model is based on the assumption that the diffuse layers around grains are interconnected in granular porous media such as sand. Hence, only the polarization of the Stern layer at the surface of the grains and the related polarization length scales can be directly associated with the size of individual grains. Charge movements related to polarization processes in the Stern layer are predominantly parallel to the grain surfaces, as slow diffusion processes hinder perpendicular movements, which implies that the dominant sizes of the corresponding polarization cells, and hence the associated SIP relaxation times, can be directly related to the prevailing grain size. Enhanced knowledge regarding such a relation between the size of polarization cells and size of grains could then pave the way to a better understanding of the potential and limitations of SIP measurements, especially, when connected to the grain-size-based permeability estimation proposed by Revil & Florsch (2010).

The data presented in this study correspond to samples of quartz sands, which vary significantly in terms of their grain size and textural characteristics and thus allow for exploring the effects of different levels of sorting and compaction on the phase amplitude in SIP (Koch *et al.* 2011). A particular emphasis of this study is to assess the impact of changes in sorting on the SIP characteristics, where sieved versions of the same original samples allows for a more direct comparison. In the following, (i) we first briefly outline the essential aspects of the mechanistic model proposed by Revil & Florsch (2010), whose practical validity we seek to test in this study, (ii) present the experimental procedures and the resulting data, and (iii) finally compare the laboratory data with the corresponding theoretical predictions.

2 ESTIMATION OF PERMEABILITY OF GRANULAR MEDIA

2.1 Grain-size-based permeability estimation

The motivation to connect the permeability to the textural parameters of a porous material is not new, the Kozeny–Carman model (Kozeny 1927; Carman 1937, 1956; Freeze & Cherry 1979) being a well known and still pertinent example. If the porous material is granular with all the grains being perfect spheres of uniform diameter d, the Kozeny–Carman equation can be written as (e.g. Freeze & Cherry 1979; Revil & Cathles 1999; Chapuis & Aubertin 2003; McCabe *et al.* 2005a,b)

$$k = \frac{d^2\phi^3}{180(1-\phi)^2}, \tag{1}$$

where k is permeability and ϕ porosity. The Kozeny–Carman model tends to overestimate the permeability, especially at low porosities, as only a fraction of the total pore space actually contributes to the medium's permeability (e.g. Revil & Cathles 1999).

To alleviate this problem, a number of authors proposed to work with parameters that are dynamically weighted by the norm of the local electrical field in the absence of surface conduction at the pore water/mineral interface (Johnson *et al.* 1986; Avellaneda & Torquato 1991)

$$k = \frac{\Lambda^2}{8F}, \tag{2}$$

where F is the formation factor and Λ is the characteristic pore size of the porous material. Archie's (1942) law then connects the formation factor to the porosity as

$$F = \phi^{-m}, \tag{3}$$

where the so-called cementation exponent m can be regarded as a grain shape parameter for granular media (Sen *et al.* 1981). According to Revil & Cathles (1999), the characteristic pore size can be quantified as by $\Lambda = d(2m(F-1))^{-1}$, which in turn allows for transforming eq. 2 to

$$k = \frac{d^2}{32m^2F\,(F-1)^2}. \tag{4}$$

This relation was then used by Revil & Florsch (2010) as the basis for their mechanistic model relating the permeability to the key SIP parameters, notably the relaxation time. Please note that eq. 4 again refers to the idealized case of perfectly spherical grains with a uniform diameter d.

2.2 Determination of permeability from SIP parameters

The resistance and the phase associated with SIP measurements can be expressed as a complex impedance, which, once corrected by a geometrical factor accounting for the experimental set-up, may be written in terms of the complex conductivity

$$\sigma^*(\omega) = \frac{1}{\rho^*(\omega)} = \sigma'(\omega) + i\sigma''(\omega) = |\sigma^*(\omega)|\exp\left(i\varphi(\omega)\right), \tag{5}$$

where ω denotes the angular frequency, ρ^* the complex resistivity, $i = \sqrt{-1}$ the imaginary number, φ the phase difference between

the injected current and the observed voltage, and σ' and σ'' the real and imaginary parts of the complex conductivity σ^*, respectively.

Revil & Florsch (2010) then use a Cole-Cole-type model for relating the distribution of the SIP relaxation times to the observed complex resistivity

$$\rho^*(\omega) = \rho_0 \left[1 - M \left(1 - \frac{1}{1 + (i\omega\tau_{CC})^c} \right) \right], \quad (6)$$

where M is the dimensionless chargeability characterizing the magnitude of the polarization effect, c is the dimensionless Cole-Cole exponent and determines the width of the peak on the corresponding phase curve with small values of c being associated with wider peaks and vice versa, τ_{CC} is the Cole-Cole time constant and is related to the location of this peak in the frequency band, and ρ_0 the low-frequency asymptote, or direct current value, of the electrical resistivity (e.g. Cole & Cole 1941; Pelton *et al.* 1978; Dias 2000; Lesmes & Friedman 2005; Cosenza *et al.* 2009). Following the original model of Schwarz (1962), for the IP relaxation time, Revil & Florsch (2010) assume that the Cole-Cole time constant τ_{CC} can be related to the square of the grain diameter d as

$$\tau_{CC} = \frac{d^2}{8D_i}, \quad (7)$$

where D_i represents the diffusion coefficient of species i in the Stern layer, which is temperature dependent and varies ∼2 per cent per degree Kelvin. For the quartz sand samples considered in this study, we shall assume that the idealized uniform grain diameter d in eq. (7) can be approximated by median grain diameter d_{50}. The pore fluid used is a sodium chloride electrolyte. Following Revil & Florsch (2010), we assume $D_{Na+} = 1.32 \times 10^{-9}$ m^2 s^{-1} at 25 °C (Tong *et al.* 2006) and an equivalent ion mobility $\beta_{Na+} = 5.19 \times 10^{-8}$ m^{2}s^{-1}V^{-1} at 25 °C (Revil *et al.* 1998) on the surface of the grains.

Assuming that the uniform diameter d in eq. (4) can be approximated by the median grain diameter d_{50}, this then results in the following relation between the permeability and SIP relaxation time

$$k = \frac{\tau_{CC} D_i}{4m^2 F(F-1)^2}. \quad (8)$$

The thus resulting proportionality between the permeability k and the relaxation time τ_{CC} was indeed already proposed by Pape & Vogelsang (1996) in relation with their work on borehole logs from the German continental deep drilling program (KTB).

3 EXPERIMENTAL BACKGROUND

The granulometric and hydraulic characteristics of the quartz sand samples considered in this study are given in Table 1. All measurements were carried out both in a loose, non-compacted state (Table 2a) as well as in a compacted state (Table 2b). The total porosity ϕ is estimated based on the observed bulk density $\delta = (1-\phi)\delta_S + \phi\delta_f$, where $\delta_s = 2650$ kg/m^3 and $\delta_f = 1000$ kg/m^3 denote the mass densities of the quartz grains and of the pore water, respectively. For all samples considered in this study, we assume the total porosity to be equal with the effective porosity.

Compaction of the samples was achieved by continued shaking and refilling of the sample holder. Vertical sorting effects, with bigger grains moving towards the surface and smaller grains accumulating at the bottom, were minimized, if not largely eliminated, by continuously changing the orientation of the vessel during the compaction process. The average difference in porosity between the non-compacted and compacted states is of the order of 7 per cent (Tables 2a and b). The compaction of the samples leaves their grain size distributions and some of their surface characteristics, such as, for example, the surface roughness of the grains, unchanged, but increases their surface area relative to the pore volume. The reduction in porosity involves a corresponding increase of the electrical formation factor F (eq. 3) of the compacted samples so that the influence of this parameter on the SIP response can be tested independently. As illustrated in Fig. 1, F is estimated by plotting the bulk conductivity of the sample as a function of the pore water conductivity. The cementation exponent m can then be inferred from the porosity ϕ and the formation factor F as $m = -\ln F / \ln \phi$. The corresponding values for F and m are given in Tables 2(a) and (b).

Table 1. Grain size characteristics from laser diffraction measurements. $u = d_{60}/d_{10}$ is the sorting of the grain size distribution. Samples SP1 to SP6 correspond to sieved fractions of sand F36 (SP1, SP2, SP3) and sand WQ1 (SP4, SP5, SP6).

Sample	d_{10} (mm)	d_{50} (mm)	d_{60} (mm)	u	Mean (mm)	Mode (mm)
F36	0.10	0.18	0.20	1.91	0.18	0.19
F32	0.18	0.27	0.29	1.62	0.27	0.27
WQ1	0.47	0.66	0.71	1.51	0.66	0.68
SP1	0.13	0.18	0.19	1.43	0.18	0.19
SP2	0.17	0.24	0.25	1.44	0.23	0.25
SP3	0.23	0.32	0.34	1.47	0.32	0.32
SP4	0.38	0.50	0.53	1.40	0.50	0.52
SP5	0.52	0.68	0.72	1.38	0.68	0.68
SP6	0.68	0.87	0.91	1.34	0.86	0.91

In addition to the original quartz sand samples, which differ in terms of their granulometric characteristics, we also consider additional samples obtained by sieving of the samples F36 and WQ1 (Table 1). The sieving resulted in six well-sorted subfractions, denoted as samples SP1 to SP6, whose SIP spectra are expected to be associated with well-defined phase peaks (Leroy *et al.* 2008; Revil & Florsch 2010). Please note that taking sieved fractions of a particular sample allows for exploring the effects of sorting on the SIP characteristics, which is a particular emphasis of this study. Because of constraints in the experimental set-up, we had to use different sample holders for the SIP and permeability measurements. This change of sample holders has the potential drawback that there can be slight differences in the underlying porosity values, although great care was taken to achieve the same final compaction state. For clarity, we denote the porosities prevailing for the permeability and SIP measurements as ϕ_k and ϕ_{SIP}, respectively (Tables 2a and b). Permeability was inferred from constant head measurements in a dedicated sample holder with a diameter 5.1 cm and a length of 5.0 cm.

The grain size distributions of our samples were determined using a Beckman Coulter LS^{TM} 13320 Laser Diffraction Particle Size Analyzer (Brea, CA), which uses an indirect method of estimating grain size via light diffraction. Based on the instrument's specifications, which conform to the ISO 13320 standards, the corresponding error margins are estimated to be 3 per cent for d_{50} and 5 per cent for d_{10}/d_{90}, respectively, with d_x referring to the grain diameter for which x per cent of the grains have a diameter smaller than this value (ISO 13320 1999).

The SIP measurements were performed using the high-accuracy impedance spectrometer developed by Zimmermann *et al.* (2008) (Fig. 2). This instrument provides an accuracy with regard to the phase of 0.1 mrad over the frequency range of interest, which extends from approximately 1 to 100 Hz. Tests under more or less identical conditions did indeed demonstrate that it was possible to closely replicate the experimental results in this frequency range

Table 2. Electrical and hydraulic parameters for (a) uncompacted and (b) compacted samples. Permeability k was measured with the constant head method at porosity ϕ_k. Porosity ϕ_{SIP} denotes the porosity measured in the sample holder used for SIP measurements using the impedance meter developed by Zimmermann *et al.* (2008) (Fig. 2). *SD* denotes the standard deviation of the various parameters as inferred from the posterior distribution resulting from the Bayesian MCMC inversion of the complex resistivity data. The electrical measurements were taken at a temperature of 21.6 °C with a standard deviation of 0.9 °C.

(a) Sample	k (m^2)	ϕ_k	F	ϕ_{SIP}	m	M	*SD M*	τ_{CC} (s)	*SD* τ_{CC} (s)	c	*SD c*
F36	1.76E-11	0.47	3.77	0.44	1.59	0.0119	0.0303	0.439	0.511	0.47	0.03
F32	5.31E-11	0.45	3.55	0.44	1.54	0.0022	0.0005	0.508	0.067	0.58	0.01
WQ1	1.29E-10	0.47	3.25	0.47	1.56	0.0232	0.0011	2.127	0.285	0.32	0.02
SP1	2.08E-11	0.48	3.14	0.46	1.48	0.0048	0.0010	0.304	0.002	0.57	0.02
SP2	3.30E-11	0.49	3.40	0.44	1.49	0.0066	0.0007	0.297	0.057	0.32	0.03
SP3	6.75E-11	0.49	3.26	0.49	1.65	0.0051	0.0007	5.133	0.585	0.47	0.02
SP4	1.71E-10	0.49	3.12	0.49	1.58	0.0063	0.0013	0.840	0.187	0.37	0.02
SP5	2.80E-10	0.48	3.10	0.48	1.54	0.0121	0.0022	4.684	1.628	0.33	0.06
SP6	3.94E-10	0.49	3.34	0.49	1.70	0.0113	0.0024	12.422	5.351	0.22	0.05
(b) Sample	k (m^2)	ϕ_k	F	ϕ_{SIP}	m	M	*SD M*	τ_{CC} (s)	*SD* τ_{CC} (s)	c	*SD c*
F36	1.11E-11	0.39	4.12	0.38	1.48	0.0232	0.0303	0.231	0.511	0.32	0.16
F32	2.40E-11	0.39	3.75	0.39	1.40	0.0038	0.0005	0.142	0.067	0.35	0.02
WQ1	7.50E-11	0.41	3.97	0.42	1.59	0.0082	0.0011	1.856	0.285	0.44	0.03
SP1	1.17E-11	0.40	3.23	0.41	1.30	0.0068	0.0010	0.142	0.002	0.50	0.02
SP2	1.98E-11	0.40	3.55	0.39	1.35	0.0050	0.0007	0.399	0.057	0.40	0.02
SP3	3.81E-11	0.42	3.64	0.42	1.49	0.0073	0.0007	5.485	0.585	0.45	0.02
SP4	1.05E-10	0.42	3.52	0.44	1.54	0.0087	0.0013	0.802	0.187	0.28	0.03
SP5	1.96E-10	0.42	3.36	0.43	1.44	0.0122	0.0022	3.654	1.628	0.33	0.05
SP6	2.56E-10	0.41	3.63	0.43	1.53	0.0080	0.0024	3.42	5.351	0.28	0.05

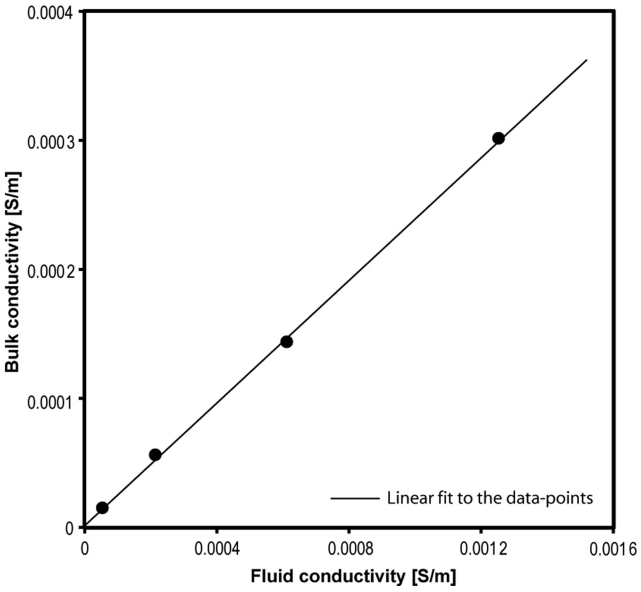

Figure 1. Bulk conductivity as a function of fluid conductivity for the compacted version of sample F36 illustrating the use of the inverse of the linear fit's slope given by $\sigma = (1/F)\sigma_f$ for estimating the formation factor F. In this example, the samples linear fit yields a value of the formation factor F of 4.1.

at different laboratories with local specimens of this impedance spectrometer (Fig. 3).

The SIP response of a probed sample provides information on the bulk electrical conductivity and the phase delay, and thus on the real and imaginary parts of the complex electrical conductivity, over the considered frequency range (eq. 5). A representative example of an observed SIP spectrum is shown in Fig. 4. Both the phase and the imaginary part of the electrical conductivity exhibit a peak at lower frequencies and a steady increase of their values for frequencies in excess of 100 Hz. The low-frequency peak is indicative of the SIP relaxation phenomena we seek to model with eq. (6). Conversely, the gradual increase of the phase and the imaginary part of the electrical conductivity at higher frequencies is related to Maxwell-Wagner polarization as well as instrument-related coupling effects (e.g. Lesmes & Morgan 2001). Repeated experiments showed that measurements in the frequency range between 1 and 10 mHz were not of the same consistency as those for higher frequencies. Similar observations have been made by other researchers (Jougnot, personal communication, 2009; Okay, personal communication, 2009). Although the causes for these problems remain enigmatic, they are likely to be related to the inherently very long measurement times associated with the low end of the SIP frequency spectrum. We recorded minor interferences with the local electricity grid in the vicinity of 50 Hz (Fig. 5).

To compare our measurements with the corresponding predictions of the model by Revil & Florsch (2010), which focuses on the low-frequency relaxation mechanism, we consider SIP spectra in the range between 10 mHz and 10 Hz and determine the Cole-Cole time constant of the so-called low-frequency peak. The only exception is sample WQ1, for which it was necessary to use frequencies down to 1 mHz, because the spectrum at higher frequencies was entirely flat. We fit the observed SIP data with the Cole-Cole model given by eq. (6) using a Bayesian Markov-chain-Monte-Carlo (MCMC) inversion approach (e.g. Mosegaard & Tarantola 1995; Chen *et al.* 2008). This approach is particularly suitable for low-dimensional, strongly non-linear problems of the type considered here and allows for a statistical assessment of the parameter estimation process based on the corresponding posterior distributions. In the absence of *a priori* information on the general characteristics, of the Cole-Cole

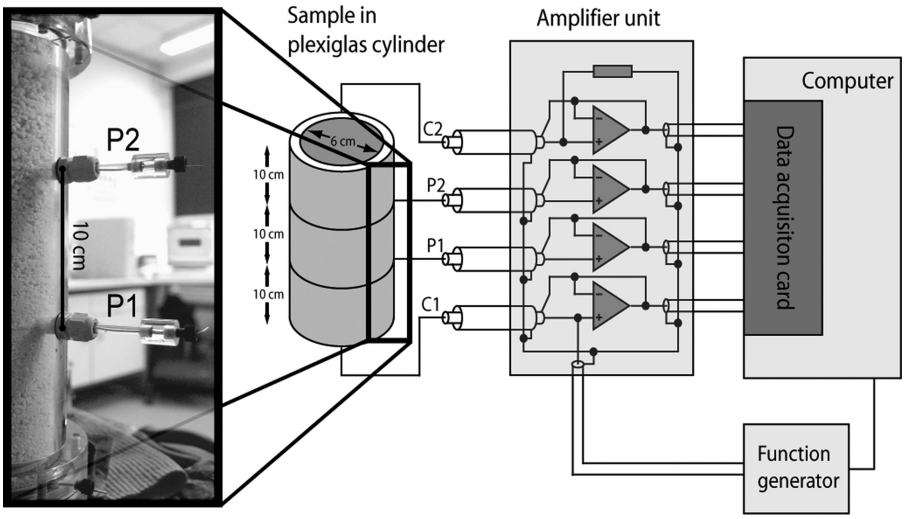

Figure 2. Sketch of the high-sensitivity impedance meter used for the SIP measurements presented in this study (adapted from Zimmermann *et al.* (2008)). The measurements are done with a Wenner-type array: C1 and C2 correspond to the current electrodes whereas P1 and P2 correspond to the potential electrodes.

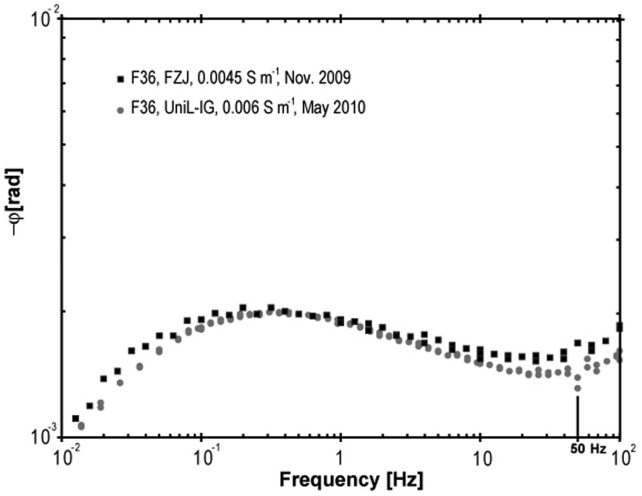

Figure 3. Results for repeated measurements of the phase φ as a function of frequency made with local specimens of the same model of the impedance spectrometer developed by Zimmermann *et al.* (2008). Black squares show the results from sample F36 measured at Forschungszentrum Jülich (FZJ) with pore water conductivity at 0.0045 S m^{-1}. Grey circles correspond to measurements made with pore water conductivity at 0.006 S m^{-1} at the Institute of Geophysics of the University of Lausanne (UniL-IG).

parameter distributions, the MCMC inversions were executed using uniform prior distributions for c and ρ_0 and log-uniform prior distributions for τ_{CC} and M. The logarithmic scale of the uniform prior distributions for τ_{CC} and M was chosen to account for the fact that likely values of these parameters may extend over several orders-of-magnitude. Table 3 gives the lower and upper ranges of the corresponding prior distributions. With the exception of the prior distribution for ρ_0, which was well constrained by the corresponding measurements of the bulk resistivity at the low end of the considered frequency spectrum, the considered prior distributions are quite broad and thus allow for assessing the information content of the SIP data with regard the Cole-Cole parameters.

We estimate the data uncertainties for the MCMC inversion procedure based on the output errors from the impedance meter, which in turn are based on repeated, threefold measurements at each frequency. The results for the mean values and the standard deviations of τ_{CC}, M, and, c are given in Tables 2(a) and (b). Another critical aspect of the MCMC procedure is to determine the length of the so-called burn-in period, the number of iterations required for the Markov chain to converge and subsequently generate samples from the Bayesian posterior distribution. Only after these first iterations are removed from the data set, the data can be used for analysis of the posterior statistics of the Cole-Cole parameters. In our case, the end of the burn-in phase, which was determined by comparing the results of three independent Markov chains with random starting points, was uniformly reached after less than 5000 iterations. After burn-in, each chain was allowed to run for 500 000 iterations, which is deemed to be largely sufficient to adequately sample the posterior distribution for this low-dimensional, four-parameter inverse problem. Representative examples of observed and fitted SIP spectra are shown in Fig. 6. Depending on the number of frequencies considered, the computations took between 1 and 5 days on a standard desktop computer with a 2.6 GHz dual core processor.

4 RESULTS

As a basis for analysing the SIP-related aspects of the model of Revil & Florsch (2010), we first need to validate the underlying relation between permeability and grain size (eq. 4). To this end, Fig. 7 shows a comparison between observed permeability data (Tables 2a and b) and the corresponding predictions based on eq. (4) (Revil & Cathles 1999), again assuming that the idealized uniform grain diameter d can be approximated by the median grain diameter d_{50} of the considered samples. For completeness, we also show of the corresponding predictions based on the Kozeny–Carman equation (eq. 1). The corresponding error estimates are based on the full differentials of the governing equations. The uncertainties of the input parameters were inferred for each sample individually and are based on the estimated errors of the various measurements involved: 3 per cent error in the measurements of grain size with the LS^{TM} 13320 Laser Diffraction Particle Size Analyzer (Beckman Coulter), ± 0.0005 kg for the scale used for weighting the samples and ± 0.0001 m accuracy of the caliper gauge for the measurement of diameter and height of the sample holder, 0.5 per cent for both fluid electric resistivity measured with the electrical conductivity meter and bulk electric resistivity measured using the SIP device.

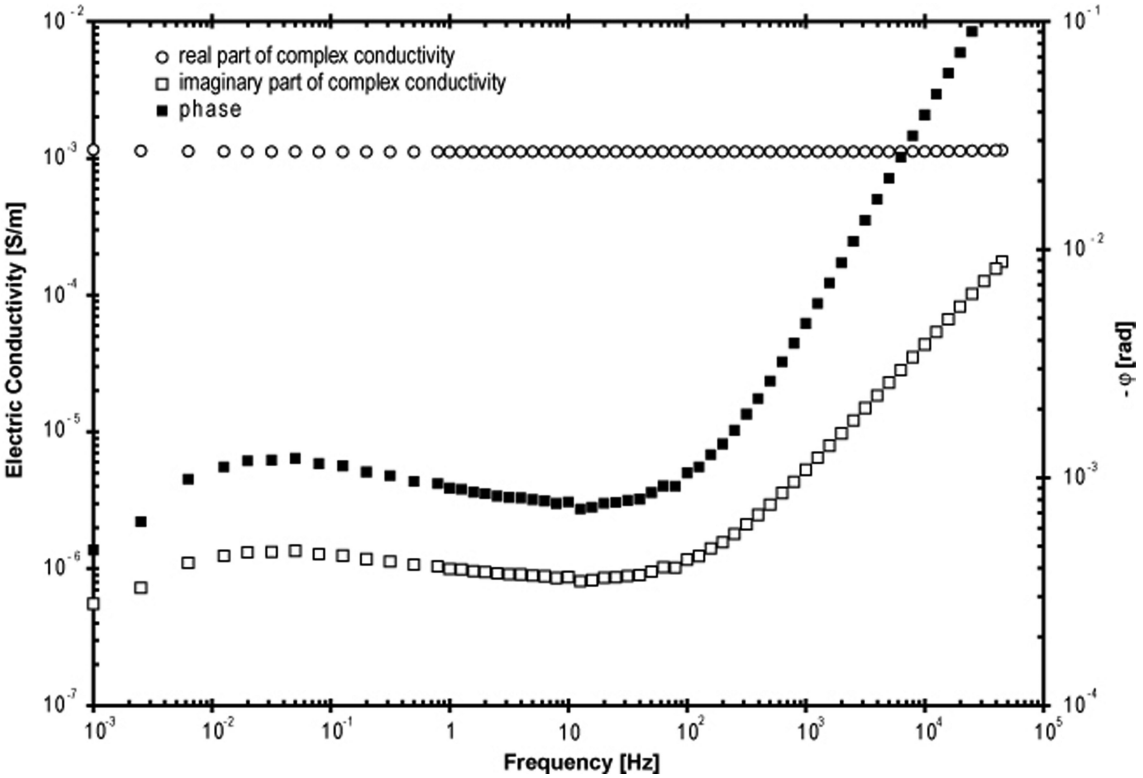

Figure 4. Example of the real and imaginary parts of the complex conductivity and corresponding phase spectra obtained from the SIP measurement of sample SP5 saturated with an NaCl electrolyte with an electrical conductivity of 0.0035 S m^{-1}. The low-frequency response of the phase and the imaginary conductivity corresponds to the polarization of the electrical double layer whereas the higher frequency responses, that is, above ∼100 Hz, are related to the effects of Maxwell-Wagner polarization (e.g. Lesmes & Morgan 2001) and instrument-related coupling effects.

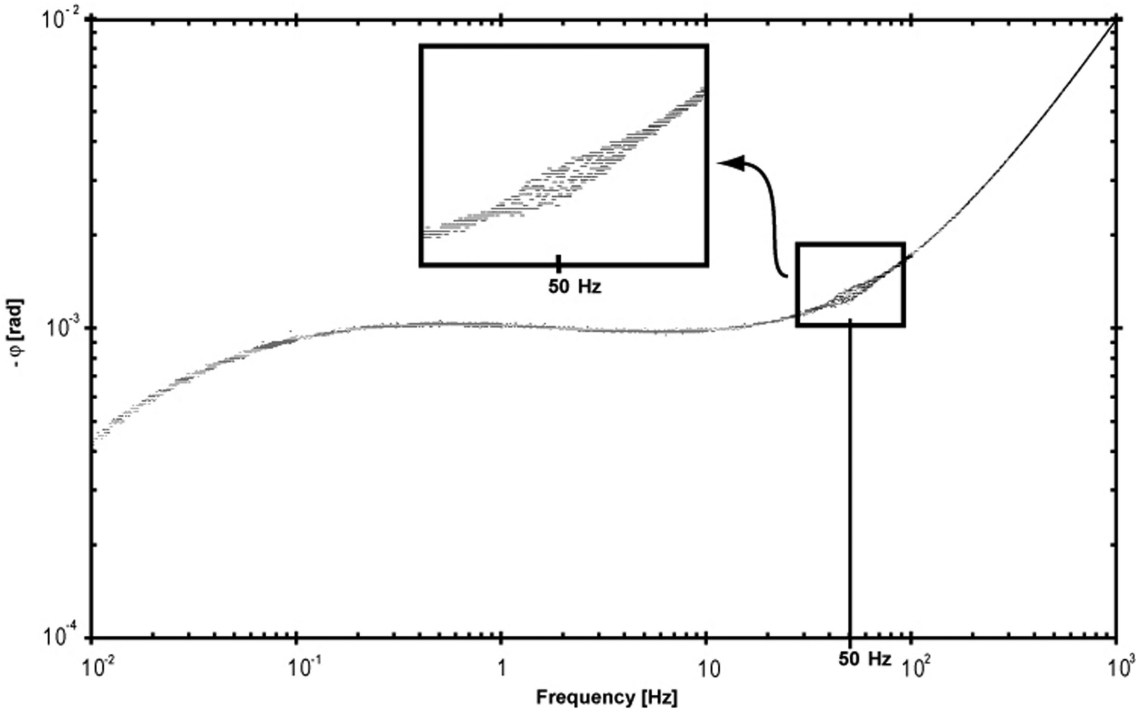

Figure 5. Zoom-in of an SIP measurement showing the typical interference effects with local electricity grid around 50 Hz.

Table 3. Lower and upper limits of the uniform (c and ρ_0) and log-uniform (M and τ_{CC}) prior distributions used for the MCMC inversion.

	Lower limit	Upper limit
c	0	0.7
ρ_0 (Ωm)	400	1100
M	0.0001	10
τ_{CC} (s)	0.00001	100

These uncertainties in the input parameters then translate into error estimates of 1.4 per cent for porosity, 1.1 per cent for the formation factor and 2.2 per cent for the cementation exponent. Please note that the formation factor is recomputed using eq. (3) at the porosities at which the permeability measurements are performed for the individual samples.

As expected, the Kozeny–Carman model (eq. 1) predicts too high values for the permeability, because it overestimates the size of the pore throats and the fraction of the pore space that controls the flow. Conversely, the model of Revil & Cathles (1999), which represents the foundation for the SIP model by Revil & Florsch (2010) based on the substitution of grain size information with SIP parameters, provides remarkably good predictions of the permeability.

In agreement with previous studies (e.g. Schwarz 1962; Binley *et al.* 2005; Leroy *et al.* 2008), we generally observe a systematic dependence of the frequency of the relaxation peaks on the grain size for our samples with smaller grains being associated with higher relaxation frequencies and *vice versa* (Fig. 8). However, an interesting, and as of yet enigmatic, difference is observed in the amplitude of phase shift between samples with the original grain size distribution (Fig. 8, black data points) and the sieved parts of the same samples (Fig. 8, coloured data points). This effect cannot be explained using currently available models and is most likely to have an influence on permeability estimations via the imaginary part of conductivity. This effect was independently observed for sample F32 by Odilia Esser at the Juelich Research Center and by the lead author for sample WQ1. In both cases, the electrical conductivity of the pore water was kept rather constant at 3–3.5 μS cm^{-1} for sample F32 and its sieved parts and at ∼50 μS cm^{-1} for sample WQ1 and its sieved parts.

Tighter packing results in a small but clearly discernible shift of the peaks of the phase (Fig. 9a) and the imaginary part of conductivity (Fig. 9b) peaks towards higher frequencies, which in turn are associated with shorter relaxation times. As this source of variation in relaxation time is not related to grain size, it will to some degree alter the permeability estimates based on eq. (8), which accounts for the impact of compaction on permeability via the formation factor (eq. 4), but does not take into account the impact of compaction on SIP relaxation time (eq. 7). Although this observation and its discrepancy with the mechanistic model of Revil & Florsch (2010) is interesting *per se*, the corresponding shifts in relaxation time are too small to have any significant implication with regard to corresponding permeability prediction. A comparison between the measured permeability values and the corresponding predictions based on eq. (8) is shown in Fig. 10. As for the grain-size-based model considered above, the formation factor was recomputed at the porosity at which the permeability measurements are performed (Tables 2a and b). The corresponding error estimates are again based on the full differential of the governing equations. The largest part of uncertainty originates from the standard deviation of the estimates relaxation times (Tables 2a and b). The errors for temperature and the electrical resistivity of the fluid of ±0.1 °K and of 0.5 per cent, respectively,

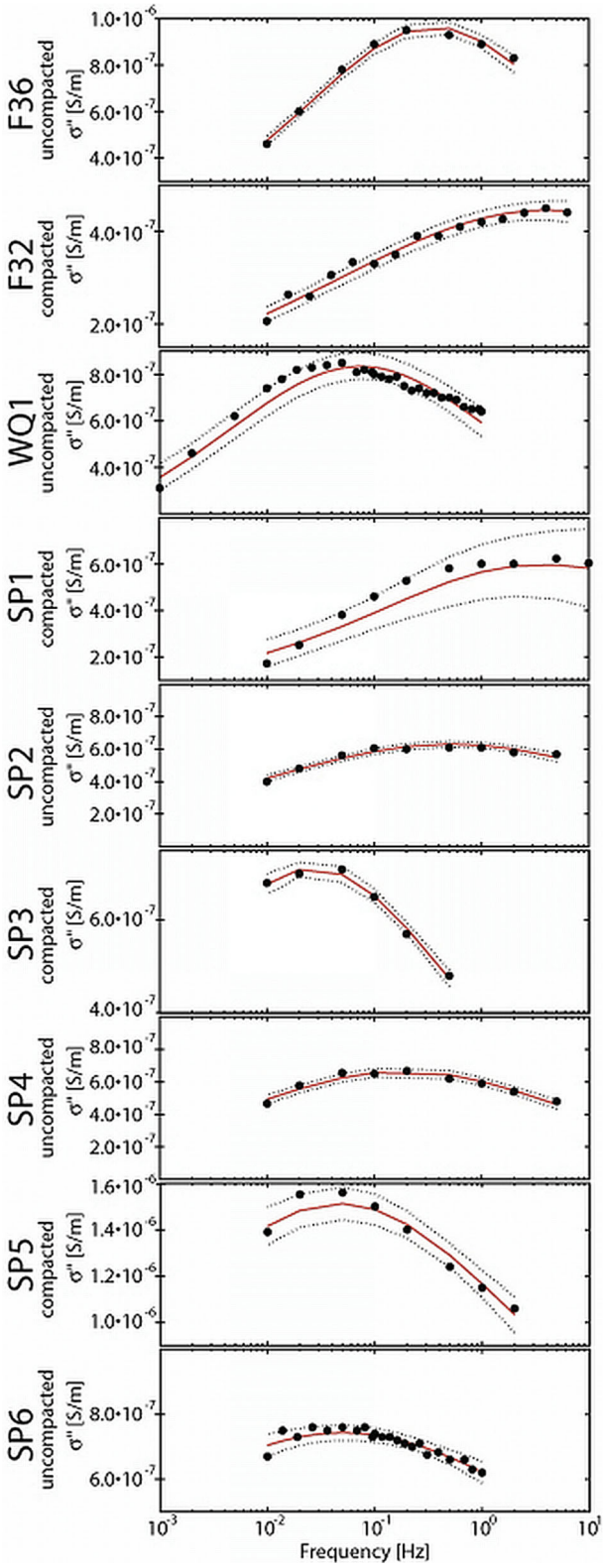

Figure 6. Examples of Cole-Cole models fitted to parts of the observed SIP data using a Bayesian MCMC inversion approach. Black dots denote the observed data, solid red lines the mean of the group of accepted models, and dashed black lines the corresponding standard deviations.

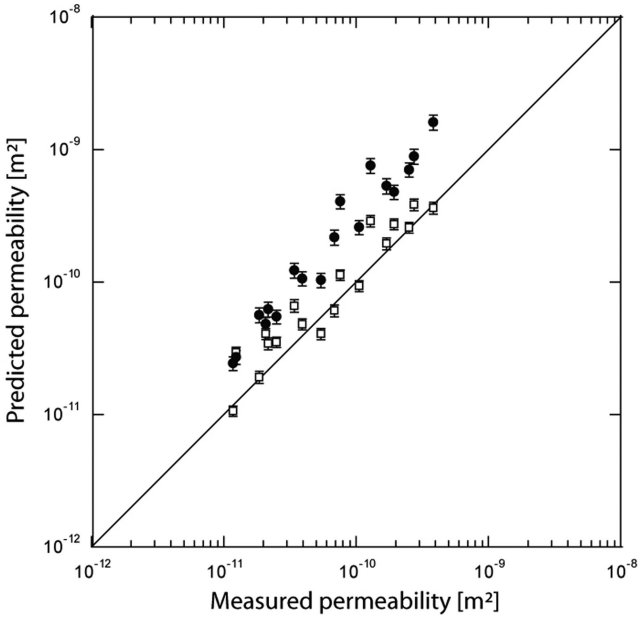

Figure 7. Predicted versus measured permeabilities comparing the Kozeny–Carman equation (eq. 1; black circles) and the Revil & Cathles (1999) model (eq. 4; open squares). As expected, the Kozeny–Carman equation overpredicts the permeability, because of its inherent overestimation of the fraction of the connected porosity. The formation factor F was computed from the cementation exponent m and the porosity ϕ_k at which the permeability is measured.

are based on the specifications of the electrical conductivity meter and its built-in thermometer meter and the error for bulk electric resistivity of 0.5 per cent correspond to the precision of the SIP device and the porosity error of 1.4 per cent is based on the full differential equations of the governing equations for our porosity estimates with a ± 0.0005 kg accuracy for the scale used for weighing the samples and ± 0.0001 m accuracy of the caliper gauge for the measurement of diameter and height of the sample holder. The latter uncertainties also contribute to the errors shown in Fig. 10, but their contribution remains relatively small in comparison with the standard deviation of the relaxation.

The results shown in Fig. 10 illustrate that eq. (8) correctly reproduces the trend of the measured permeabilities, but systematically underpredicts their actual values by approximately one order-of-magnitude, which is indeed within the common uncertainty range associated with predictions and measurements of permeability. However, there are also indications, such as the dependence of the relaxation times on compaction, that some of the rather strong assumptions inherent to the model of Revil & Florsch (2010), such as its focus on the polarization of the Stern layer, could be at the source of this observation.

5 DISCUSSION

A seemingly obvious candidate for explaining the systematic underprediction of the observed permeability would be a corresponding error in the diffusion coefficient (eq. 8). Indeed, previous workers have put forward the idea of using the diffusion coefficient as a fitting parameter for closely related problems (e.g. Schwarz 1962). In our case, this approach would, however, lead to values of ion mobility that exceed those used in related works by one order-of-magnitude (e.g. Leroy *et al.* 2008). This discrepancy is quite unrealistic and thus indicates that fundamental inadequacies in the underlying mechanistic model, rather than inaccuracies in the estimation of the diffusion coefficient, are likely to be at the source of the mismatch between the observed and the modelled permeabilities.

For the following, it is therefore important to remember that the model by Revil & Florsch (2010) is essentially based on the assumption that the polarization process is dominated by the Stern layer. In the given context, this dominance of the Stern layer implies that the diffuse layer is assumed to be interconnected over the entire pore space and hence polarization processes taking place in the diffuse layer are not considered in the model. Notably membrane polarization, which is widely regarded as an important polarization mechanism (e.g. Marshall & Madden 1959; Vinegar & Waxman 1984; de Lima & Sharma 1992; Lesmes & Morgan 2001; Titov *et al.* 2002) and is not accounted for by this model. Not accounting for the polarization processes in the diffuse layer may indeed result in a systematic underestimation of the observed permeability by the corresponding SIP-based model (eq. 8). The fact that the underlying grain-size-based model (eq. 4) predicts the observed permeability of our samples quite adequately supports this view.

To explain the systematic underprediction of the observed permeability by this model, we therefore need to look for realistic, but unaccounted, polarization mechanisms, which cause the observed SIP relaxation times to be shorter than would be expected from the Stern layer polarization of individual spherical grains. Quite importantly, these polarization mechanisms should also be compatible with our observation that compaction of the samples results in a small but systematic reduction of their Cole-Cole time constants (Tables 2a and b).

As described above, an important polarization mechanism in porous media, which works in this direction and which is not accounted for in the considered model, is membrane polarization, which is commonly associated with the pore length (e.g. Volkmann & Klitzsch 2010). The pore length in unconsolidated granular media is generally smaller than the average diameter of the surrounding grains and hence is likely to be associated with systematically shorter relaxation times than those assumed by the model of Revil & Florsch (2010). Moreover, compaction tends to further reduce the pore length, which in turn is compatible with our observation that the compacted samples exhibit systematically shorter relaxation times than their non-compacted, loose counterparts (Tables 2a and b).

In the context of this study, it is also important to remember that the individual grains of our quartz sand samples differ quite significantly in terms of their shape and their surface roughness from the underlying assumption on ideal spheres (Fig. 11). These shape characteristics might allow for the development of multiple polarized cells on the surfaces of the individual grains. In well-controlled laboratory experiments involving spherical glass beads, Leroy *et al.* (2008) did indeed observe that edging of the beads resulted in the development of additional smaller polarized cells in response to the corresponding increase of the surface roughness. Although this process can be explained based on the Stern layer polarization processes, it is not accounted for in the current model of Revil & Florsch (2010).

Moreover, the size of the polarized cells may also be reduced with respect to the considered Stern-layer-based model as a result of contacts between the electrical double layers surrounding the individual grains. This phenomenon and its effects on the governing polarization mechanisms are not well understood and have only been studied with regard to spheres in suspension (e.g. Dukhin & Shilov

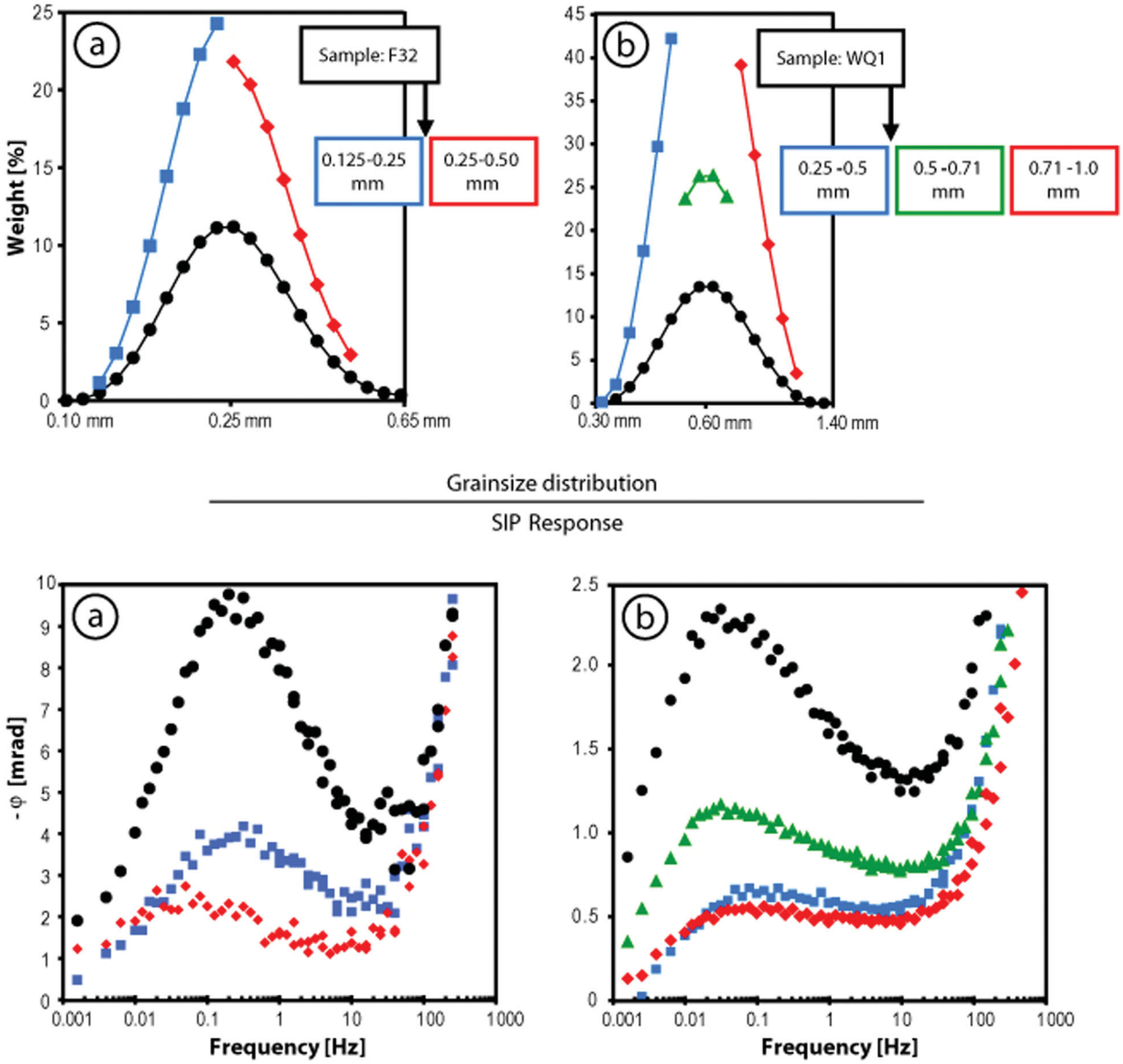

Figure 8. Granulometry (top) and SIP responses (bottom) of (a) sample F32 and two sieved fractions thereof at a pore water conductivity of 3 to 3.5 μS cm^{-1} and (b) sample WQ1 and three sieved fractions thereof at pore water conductivity of ∼50 μS cm^{-1}. In both cases, we observe a significantly smaller amplitude of the phase φ for the well sorted, sieved fractions (coloured data points) of the samples than for the original grain size distribution (black circles) of the samples.

1969, 1974, 2001; Shilov *et al.* 2001; Grosse 2011). It has, however, been shown that the distance between particles in suspension has an effect on polarization processes and that the relaxation times do indeed decrease with increasing particle concentration (e.g. Schwan *et al.* 1962; Shilov & Borkovskaja 1994; Delgado *et al.* 1998). If the correspondingly reduced size of the polarized cells is linked to the distance between contacts of multiple individual grains, we can assume it to be similar to the pore length in unconsolidated granular media and thus to be similar to the size of the polarization cells associated with membrane polarization. In this context, it is interesting to note that the recently proposed hydraulic model of Bernabe *et al.* (2010, 2011) does indeed use the pore length l together with the hydraulic radius r_H as the key parameters for permeability estimation.

Finally, it also important to remember that the decrease in porosity as a result of compaction is associated with a corresponding increase of the tortuosity $T = F\phi = \phi^{1-m}$ (Clennell 1997). Together with recent findings of Binley *et al.* (2010) for sandstone samples, which indicate a linear relationship between the square root of the tortuosity and the relaxation length scale, this may point to the possibility and/or the necessity of correcting Revil & Florsch's (2010) mechanistic model for the tortuosity. That said, the corresponding variations of the formation factor remain relatively small for our samples and hence the formation factor would need to be multiplied by four to adequately represent compaction related variations in relaxation time.

6 CONCLUSIONS

We explored the practical validity of the mechanistic model based on the polarization of the Stern layer proposed by Revil & Florsch

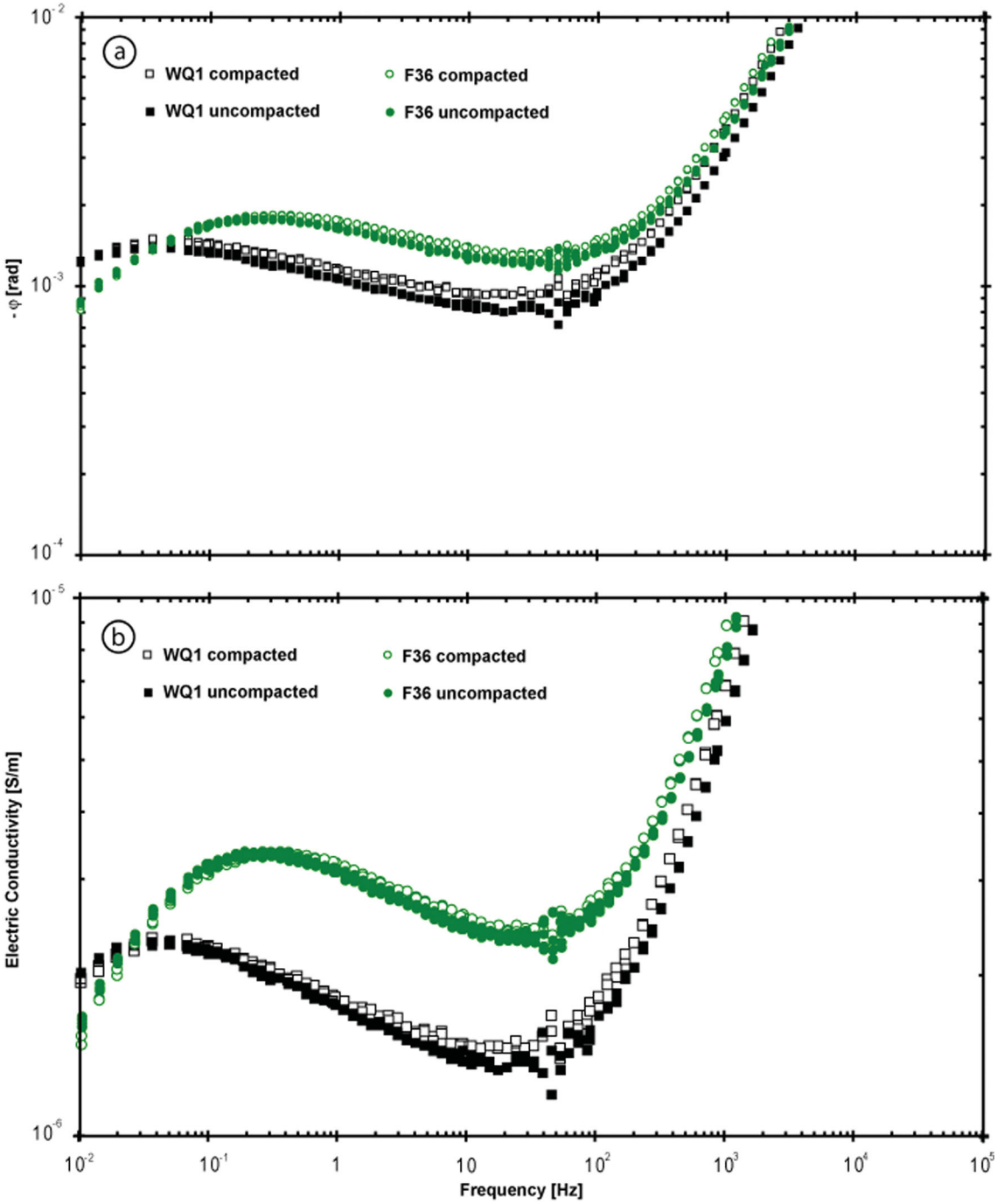

Figure 9. Effect of compaction on (a) the phase φ and (b) the imaginary part of the electrical conductivity for samples WQ1 and F36.

(2010) relating SIP relaxation time to the mean grain size and the permeability. To this end, we compared the theoretical predictions with corresponding laboratory measurements for quartz sands with relatively broad and varying granulometric characteristics. The grain-size-based model, upon which the SIP model considered in this study is based, predicts the permeability very adequately. Correspondingly, we attribute the observed discrepancies arising in the permeability prediction from the SIP relaxation time to inadequacies in the part of the model concerning polarization processes. The trend of the permeability predictions based on the observed Cole-Cole time constants inferred from SIP data agrees well with the corresponding measured data. The model does, however, systematically underestimate the observed permeability values by approximately one order-of-magnitude. Although the magnitude of this systematic mismatch is within the common uncertainty range associated with predictions and measurements of this inherently elusive hydraulic parameter, there are indications, such as the dependence of the relaxation times on compaction, that some of the rather strong assumptions inherent to this model, such as its limitation to the polarization of the Stern layer, could be at the source of this observation. From a practical point of view, the effects of compaction seem to be negligible for the prediction of permeability

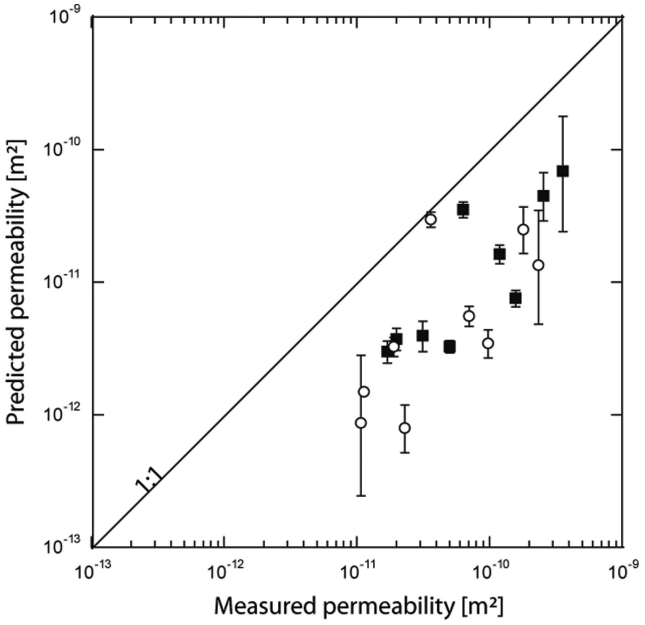

Figure 10. Predicted (eq. 8) versus measured permeabilities using the mean Cole-Cole time constant based on the spectral induced polarization data, the formation factor and the cementation exponent. The results for compacted and loose, non-compacted samples are displayed as open circles and solid black squares, respectively.

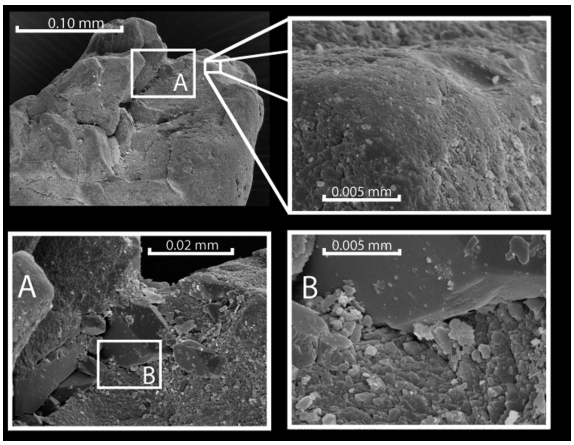

Figure 11. Electron microscope images of a quartz sand grain from sample F32 at various levels of magnification.

from SIP data. However, the very observation of this effect points to the existence and the potential importance of polarization processes that are not accounted for in the considered model, such as, for example, membrane polarization and/or the presence of multiple and hence smaller polarized cells in response to surface roughness and intergrain contacts.

ACKNOWLEDGMENTS

This research has been supported by a grant from the Swiss National Science Foundation. AR thanks the National Science Foundation for the support of the project 'Spectral Induced Polarization to invert permeability' (NSF award NSF EAR-0711053), whose results fertilized this study. We thank Harry Vereecken and the Forschungszentrum Juelich for facilitating collaborations. Special thanks go to Sander Huisman, Egon Zimmermann, Odilia Esser, Franz-Hubert Haegel, Katrin Breede, Marie Scholer and James Irving for their help with various aspects of this project and to Quarzwerke Frechen for providing the samples used in this study. We also gratefully acknowledge the thorough and constructive reviews by Jörg Renner (editor), Andrew Binley, Lee Slater, and an anonymous referee as well as fruitful discussions with Andreas Kemna and Damien Jougnot.

REFERENCES

Annan, A.P., 2005. GPR methods for hydrological studies, in *Hydrogeophysics,* pp. 185–213, eds Rubin, Y. & Hubbard, S., Springer, Dordrecht.

Archie, G.E., 1942. The electrical resistivity log as an aid in determining some reservoir characteristics, *Trans. Am. Inst. Min. Metall. Eng.,* **146,** 54–61.

Avellaneda, M. & Torquato, S., 1991. Rigorous link between fluid permeability, electrical conductivity, and relaxation times for transport in porous media, *Phys. Fluids,* **3,** 2529–2540.

Bernabe, Y., Li, M. & Maineult A., 2010. Permeability and pore connectivity: a new model based on network simulations, *J. geophys. Res.,* **115,** B10203, doi:10.1029/2010JB007444.

Bernabe, Y., Zamora, M., Li, M., Maineult, A. & Tang Y., 2011. Pore connectivity, permeability and electrical formation factor: a new model and comparison to experimental data, *J. geophys. Res.,* **116,** B11204, doi:10.1029/2011JB008543.

Binley, A. & Kemna, A., 2005. DC resistivity and induced polarization methods, in *Hydrogeophysics,* pp. 129–156, eds Rubin, Y. & Hubbard, S., Springer, Dordrecht.

Binley, A., Slater L., Fukes M. & Cassiani, G., 2005. The relationship between spectral induced polarization and hydraulic properties of saturated and unsaturated sandstone, *Water Resour. Res.,* **41,** W12417, doi:10.1029/2005WR004202.

Binley, A., Kruschwitz, S., Lesmes, D. & Kettridge, N., 2010. Exploiting the temperature effects on low-frequency electrical spectra of sandstone: A comparison of effective diffusion path lengths, *Geophysics,* **75**(6), A43–A46, doi:10.1190/1.3483815.

Börner, F.D., Schopper, J.R. & Weller, A., 1996. Evaluation of transport and storage properties in the soil and groundwater zone from induced polarization measurements, *Geophys. Prospect.,* **44,** 583–601.

Carman, P.C., 1937. Fluid flow through granular beds, *Trans. Inst. Chem. Eng.,* **15,** 150–166.

Carman, P.C., 1956. *Flow of Gases Through Porous Media,* Butterworths Scientific Publications, London.

Chapuis, R.P. & Aubertin, M., 2003. Predicting the coefficient of permeability of soils using the Kozeny-Carman equation. Report EPM–RT–2003–03, Département des génies civil, géologique et des mines; École Polytechnique de Montréal, 2003 January. Available at: http://www.polymtl.ca/biblio/epmrt/rapports/rt2003-03.pdf (last accessed 2012 May 3).

Chen, J., Kemna, A. & Hubbard, S., 2008. A comparison between Gauss-Newton and Markov-chain Monte Carlo-based methods for inverting spectral induced-polarization data for Cole-Cole parameters, *Geophysics,* **73,** F247–F259, doi:10.1190/1.2976115.

Clennell, M.B., 1997. Tortuosity: a guide through the maze, in *Developments in Petrophysics,* Geol. Soc. London Spec. Pub., Vol. 122, pp. 239–344, eds Lovell, M.A. & Harvey, P.K., Geological Society, London.

Cole, K.S. & Cole, R.H., 1941. Dispersion and absorption in dielectrics I. Alternating current characteristics, *J. Chem. Phys.,* **9,** 341–351.

Cosenza, P., Ghorbani, A., Camerlynck, C., Rejiba, F., Guérin, R. & Tabbagh, A., 2009. Effective medium theories for modelling the relationships between electromagnetic properties and hydrological variables in geomaterials: a review, *Near Surf. Geophys.,* **7,** 563–578, doi:10.3997/1873-0604.2009009.

de Lima, O.A.L. & Sharma, M.M., 1992. A generalized Maxwell-Wagner theory for membrane polarization in shaly sands, *Geophysics,* **57,** 431–440.

Delgado, A.V., Arroyo, F.J., Gonzales-Caballero, F., Shilov, V.N. & Borkovskaya, Y.B., 1998. The effect of the concentration of dispersed particles on the mechanisms of low-frequency dielectric dispersion (LFDD) in colloidal suspensions, *Colloids Surf.,* **140,** 139–149, doi:10.1016/S0927-7757(9)00272-0.

Dias, C.A., 2000. Developments in a model to describe low-frequency electrical polarization of rocks, *Geophysics,* **65,** 43–451.

Domenico, P.A. & Schwartz, F.W., 1998. *Physical and Chemical Hydrology,* p. 506, John Wiley & Sons, New York.

Dukhin, S.S. & Shilov, V.N., 1969. Theory of the static polarization of the diffuse part of the thin double layer of spherical particles, *Kolloidn. Zh.,* **31,** 706–713.

Dukhin, S.S. & Shilov, V.N., 1974. *Dielectric Phenomena and the Double Layer in Dispersed Systems and Polyelectrolytes,* p. 34, John Wiley & Sons, New York.

Dukhin, S.S. & Shilov, V.N., 2001. *Interfacial Electrokinetics and Electrophoresis,* pp. 55–85, ed. Delgado, A.V., Marcel Dekker, New York.

Freeze, A.R. & Cherry, A., 1979. *Groundwater,* p. 640, Prentice-Hall, Englewood Cliffs, NJ.

Gelhar, L.W., 1993. *Stochastic Subsurface Hydrology,* p. 390, Prentice-Hall, Englewood Cliffs, NJ.

Grosse, C., 2011. Extension of a classic thin double layer polarization theory of colloidal suspensions to include the stagnant layer conductivity, *J. Phys. Chem.,* **115,** 8994–9004.

Hördt, A., Blaschek, R., Kemna, A. & Zisser, N., 2007. Hydraulic conductivity estimation from induced polarization data at the field scale—the Krauthausen case history, *J. appl. Geophys.,* **62,** 33–46.

Hubbard, S.S. & Linde, N., 2011. Hydrogeophysics, in *Treatise on Water Science,* pp. 401–434, ed. Wilderer, P.H., Elsevier, Amsterdam.

ISO 13320, 1999. *Particle Size Analysis—Laser Diffraction Methods*, International Organization for Standardization, Geneva.

Johnson, D.L., Plona, T.J. & Kojima, H., 1986. Probing porous media with 1st sound, 2nd sound, 4th sound and 3rd sound, in *Physics and Chemistry of Porous Media,* pp. 243–277, Vol. 2, eds Jayanth, R., Banavar, J. & Winkler, K.W., AIP, New York, NY.

Kemna, A., Binley, A. & Slater, L., 2004. Crosshole IP imaging for engineering and environmental applications, *Geophysics,* **69,** 97–107.

Koch, K., Wenninger, J., Uhlenbrook, S. & Bonell, M., 2009. Joint interpretation of hydrological and geophysical data: electrical resistivity tomography results from a process hydrological research site in the Black Forest Mountains, Germany, *Hydrol. Process.,* **23,** 1501–1513.

Koch, K., Kemna, A., Irving, J. & Holliger, K., 2011. Impact of changes in grain size and pore space on the hydraulic conductivity and spectral induced polarization response of sand, *Hydrol. Earth Syst. Sci.,* **15,** 1785–1794, doi:10.5194/hess-15-1785-2011.

Kormiltsev, V.V., 1963. O vozbuzdenii I spade vyzvannoi polarizatsii v kapillarnoi srede (On excitation and decay of Induced Polarization in capillary medium), *Izvestia AN SSSR, Seria Geofizicheskaya* (*Solid Earth Phys.*), **11,** 1658–1666 [in Russian].

Kozeny, J., 1927. Ueber kapillare Leitung des Wassers im Boden, Wien, *Akad. Wiss.,* **136**(2a), 271–306 (in German).

Leroy, P., Revil, A., Kemna, A., Cosenza, P. & Gorbani, A., 2008. Spectral induced polarization of water-saturated packs of glass beads, *J. Colloid Interface Sci.,* **321**(1), 103–117.

Lesmes, D.P. & Morgan, F.D., 2001. Dielectric spectroscopy of sedimentary rocks, *J. geophys. Res.,* **106,** 13 329–13 346.

Lesmes, D.P. & Friedman S., 2005. Relationships between electrical and hydrogeological properties of rocks and soils, in *Hydrogeophysics,* pp. 129–156, eds Rubin, Y. & Hubbard, S., Springer, Dordrecht.

Linde, N., Binley, A., Tryggvason, A., Pedersen, L.B. & Revil, A., 2006. Improved hydrogeophysical characterization using joint inversion of crosshole electrical resistance and ground penetrating radar traveltime data, *Water Resour. Res.,* **42,** W12404, doi:10.029/2006WR005131.

Malama, B., Revil, A. & Kulhman, K.L., 2009a. A semi-analytical solution for transient streaming potentials associated with confined aquifer pumping tests, *Geophys. J. Int.,* **176,** 1007–1016, doi:10.1111/j.1365-246X.2008.04014.x.

Malama, B., Kuhlman, K.L. & Revil, A., 2009b. Theory of transient streaming potentials associated with axial-symmetric flow in unconfined aquifers, *Geophys. J. Int.,* **179,** 990–1003, doi:10.1111/j.1365-246X.2009.04336.x.

Marshall, D.J. & Madden, T.R., 1959. Induced polarization: a study of its causes, *Geophysics,* **24,** 790–816.

McCabe, W.L., Smith, J.C. & Harriot, P., 2005a. *Unit Operations of Chemical Engineering,* 7th edn, pp. 163–165, McGraw-Hill, New York, ISBN 0-07-284823-5.

McCabe, W.L., Smith, J.C. & Harriot, P., 2005b. *Unit Operations of Chemical Engineering,* 7th edn, p. 188–189, McGraw-Hill, New York, ISBN 0-07-284823-5.

Mosegaard, K. & Tarantola, A., 1995. Monte Carlo sampling of solutions to inverse problems, *J. geophys. Res.,* **100,** 12 431–12 447, doi:10.1029/94JB03097.

Pape, H. & Vogelsang, D., 1996. Fractal evaluation of induced polarization logs in the KTB-Oberpfalz HB: Bundesanstalt für Geowissenschaften und Rohstoffe / Geologische Landesämter in der Bundesrepublik Deutschland, *Geologisches Jahrbuch,* **54**(E), 3–27.

Pelton, W.H., Ward S.H., Hallof, P.G., Sill, W.R. & Nelson, P.H., 1978. Mineral discrimination and removal of inductive coupling with multifrequency IP, *Geophysics,* **43,** 588–609.

Revil, A., Cathles, L.M. & Losh, S., 1998. Electrical conductivity in shaly sands with geophysical applications, *J. geophys. Res.,* **103,** 925–936.

Revil, A. & Cathles, L.M., 1999. Permeability of shaly sands, *Water Resour. Res.,* **35**(3), 651–662.

Revil, A. & Florsch, N., 2010. Determination of permeability from spectral induced polarization in granular media, *Geophys. J. Int.,* **181** (3), 1480–1498, doi:10.1111/j.1365-246X.2010.04573.x.

Revil, A., Woodruff, W.F. & Lu, N., 2011. Constitutive equations for coupled flows in clay materials, *Water Resour. Res.,* **47,** W05548, doi:10.1029/2010WR010002.

Robinson, D.A. *et al*., 2008. Advancing process-based watershed hydrological research using near-surface geophysics: a vision for, and review of, electrical and magnetic geophysical methods, *Hydrol. Process.,* **22** (18), 3604–3635, doi:10.1002/hyp.6963.

Rubin, Y. & Hubbard, S. (eds), 2005. *Hydrogeophysics,* p. 523, Springer, Dordrecht.

Schwan, H.P., Schwarz, G., Maczuk, J. & Pauly, H., 1962. On the low-frequency dielectric dispersion of colloidal particles in electrolyte solution, *J. Phys. Chem.,* **66,** 2626–2635, doi:10.1021/j100818a066.

Schwarz, G., 1962. A theory of the low-frequency dispersion of colloidal particles in electrolyte solution, *J. Phys. Chem.,* **66,** 2636–2642.

Sen, P.N., Scala, C. & Cohen, M.H., 1981. A self-similar model for sedimentary rocks with application to the dielectric constant of fused glass beads, *Geophysics,* **46**(5), 781–795.

Shilov, V.N. & Borkovskaja, Y.B., 1994. *Kolloidn Zh*., **56,** 647 (in Russian).

Shilov, V.N., Delgado, A.V., Gonzalez-Caballero, F. & Grosse, C., 2001. Thin double layer theory of the wide-frequency range dielectric dispersion of suspensions of non-conducting spherical particles including surface conductivity of the stagnant layer, *Colloids Surf.,* **192,** 253–265.

Slater, L. & Lesmes, D.P., 2002. Electrical-hydraulic relationships observed for unconsolidated sediments, *Water Resour. Res.,* **38,** 1213, doi:10.1029/2001WR001075.

Slater, L., 2007. Near surface electrical characterization of hydraulic conductivity: from petrophysical properties to aquifer geometries—a review, *Surv. Geophys.,* **28,** 169–197.

Stingaciu, L.R., Weihermüller, L., Haber-Pohlmeier, S., Stapf, S., Vereecken, H. & Pohlmeier, A., 2010. Determination of pore size distribution and hydraulic properties using nuclear magnetic resonance relaxometry: a comparative study of laboratory methods, *Water Resour. Res.,* **46,** W11510, doi:10.1029/2009WR008686.

Titov, K., Komarov, V., Tarasov, V. & Levitski, A., 2002. Theoretical and experimental study of time-domain induced polarization in water saturated sands, *J. appl. Geophys.,* **50,** 417–433.

Titov, K., Kemna, A., Tarasov, A. & Vereecken, H., 2004. Induced polarization of unsaturated sands determined through time domain measurements, *Vadose Zone J.,* **3,** 1160–1168.

Tong, M., Li, L., Wang, W. & Jiang, Y., 2006. A time-domain induced-polarization method for estimating permeability in a shaly sand reservoir, *Geophys. Prospect.,* **54,** 623–631.

Vinegar, H.J. & Waxman, M.H., 1984. Induced polarization of shaly sands, *Geophysics,* **49,** 1267–1287.

Volkmann, J. & Klitzsch, N., 2010. Frequency-dependent electric properties of microscale rock models for frequencies from one millihertz to ten kilohertz, *Vadose Zone J.,* **9,** 858–870, doi:10.2136/vzj2009.0162.

Weller, A., Nordsiek, S. & Debschütz, W., 2010. Estimating permeability of sandstone samples by nuclear magnetic resonance and spectral-induced polarization, *Geophysics,* **75,** 215–226, doi:10.1190/1.3507304.

Zimmermann, E., Kemna, A., Berwix, J., Glaas, W., Muench, H.M. & Huisman, J.A., 2008. A high-accuracy impedance spectrometer for measuring sediments with low polarizability, *Meas. Sci. Technol.,* **19,** 105603, doi:10.1088/0957-0233/19/10/105603.